Vortices in self-bound dipolar droplets

André Cidrim,[1,2] Francisco E. A. dos Santos,[1] Emanuel A. L. Henn,[2] and Tommaso Macrì[3]

[1]*Departamento de Física, Universidade Federal de São Carlos, 13565-905 São Carlos, São Paulo, Brazil*
[2]*Instituto de Física de São Carlos, Universidade de São Paulo, C.P. 369, 13560-970 São Carlos, SP, Brazil*
[3]*Departamento de Física Teórica e Experimental, Universidade Federal do Rio Grande do Norte,
and International Institute of Physics, Natal-RN, Brazil*

Quantized vortices have been observed in a variety of superfluid systems, from ^{4}He to condensates of alkali-metal bosons and ultracold Fermi gases along the BEC-BCS crossover. In this article we study the stability of singly quantized vortex lines in dilute dipolar self-bound droplets. We first discuss the energetic stability region of dipolar vortex excitations within a variational ansatz in the generalized nonlocal Gross-Pitaevskii functional that includes quantum fluctuation corrections. We find a wide region where stationary solutions corresponding to axially symmetric vortex states exist. However, these singly charged vortex states are shown to be unstable, either by splitting the droplet in two fragments or by vortex-line instabilities developed from Kelvin-wave excitations. These observations are the results of large-scale fully three-dimensional simulations in real time. We conclude with some experimental considerations for the observation of such states and suggest possible extensions of this work.

I. INTRODUCTION

Quantized vortices are a direct manifestation of the genuine quantum behavior of superfluid systems. A prime example is superfluid helium, which has been widely studied over the past decades. Ultracold quantum gases offer the possibility to investigate vortex properties in a complementary regime in terms of particle numbers, interaction strength, and range [1,2] with either bosonic [3] or fermionic [4] atoms. Dipolar condensates may also display vortex excitations with peculiar properties as a consequence of the long range and anisotropy of the interactions [5–8]. For a three-dimensional condensate with a vortex line and in the presence of a periodic potential, the spectrum of transverse modes may display a rotonlike minimum [9,10], which destabilizes the straight vortex and leads to a transition from vortex into helical or snakelike configurations [11,12].

Theoretical models of superfluid states of ultracold gases at zero temperature are usually based on well-established mean-field approximations which accurately describe experiments [13], ranging from analytic treatments and variational approaches to full numerical simulations. Corrections beyond the mean-field picture have been measured for strongly interacting Bose gases [14] and for ultracold fermions along the BCS-BEC crossover [15] and compared with *ab initio* quantum Monte Carlo calculations.

The recent observation of ultradilute self-bound droplets both in dipolar condensates [16–22], as well as in two-component Bose mixtures [23], together with a combined theoretical effort, established the importance of the fundamental role of quantum fluctuations in ultracold atomic systems [24–38]. Yet, no work has investigated the presence and stability of vortex states in self-bound droplets in ultradilute liquids.

Helium droplets hosting several quantized vortices have been recently observed [39] and studied in detail theoretically [40–43], both in pure samples and in the presence of impurities.

The scales are, nevertheless, completely different. Helium droplets can be easily taken as a homogeneous, infinite superfluid background since vortices are much smaller compared to the system size (given the large interaction strengths).

Droplets in quantum ferrofluids are very anisotropic, and vortex cores are expected to have a size comparable to that of the whole droplet. Here we address the issue of stability and dynamics of singly quantized vortex lines in dipolar droplets for a wide range of dipolar interaction strengths and particle numbers. We carry out large-scale fully three-dimensional simulations, which allow for an efficient determination of energies and shapes of droplets as well as their dynamics. We find a strong anisotropy of such droplets, very elongated along the polarization axis. For small particle numbers, droplets are dynamically unstable towards splitting in two droplets where angular momentum is redistributed into surface collective excitations [44]. For larger sizes we do not observe splitting, yet vortex lines display bending for long times [12,45–48]. We conclude with a discussion of a possible experimental implementation and observation of our findings with current experimental setups.

II. METHODS

The dynamics of an untrapped dipolar Bose-Einstein condensate is described by a generalized nonlocal Gross-Pitaevskii equation,

$$i\hbar\dot{\psi} = \left(-\frac{\hbar^2\nabla^2}{2m} + \mathcal{K}_{\rm int}(\mathbf{r}) + g_{\rm LHY}|\psi|^3\right)\psi, \quad (1)$$

where $\psi(\mathbf{r},t)$ is the BEC wave function. $\mathcal{K}_{\rm int}(\mathbf{r}) = g_c|\psi(\mathbf{r})|^2 + \int d\mathbf{r}'\, V_{\rm dd}(\mathbf{r}-\mathbf{r}')|\psi(\mathbf{r}')|^2$ describes the contact and dipolar mean-field interaction of the condensate. Here $g_c = 4\pi a_s\hbar^2/m$ is the contact interaction strength, with a_s being the s-wave scattering length, and $V_{\rm dd}(\mathbf{r}) = \frac{C_{\rm dd}}{4\pi}\frac{1-3\cos^2\theta}{r^3}$
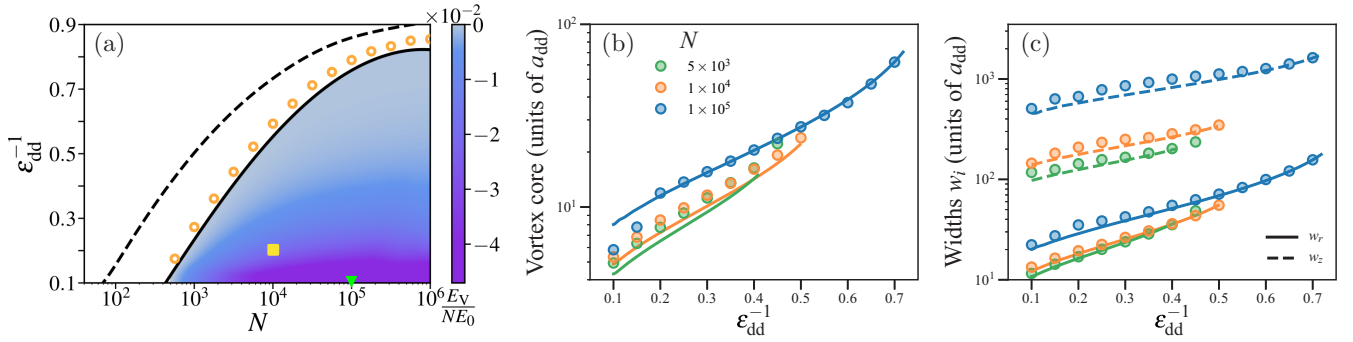
FIG. 1. (a) Stability diagram of an axisymmetric droplet with a vortex line. Density plot of the energy per particle of self-bound solutions hosting a vortex as a function of ε_{dd}^{-1} and N calculated using the variational Gaussian wave function (2). The thick black line corresponds to $E_V = 0$. Energy is in units of $E_0 = \hbar^2/(m\, a_{dd}^2)$. The yellow square and the green triangle correspond to $(N, \varepsilon_{dd}^{-1}) = (10^4, 0.2)$ and $(10^5, 0.1)$ coordinates, respectively, used in Fig. 2 to characterize the dynamics. (b), (c) Characterization of droplets hosting a vortex line. (b) Size of the vortex core scaled by the dipolar length as a function of ε_{dd}^{-1} and for $N = 5 \times 10^3, 10^4, 10^5$ particle numbers. Full dots correspond to energy minima of the Gross-Pitaevskii energy functional. (c) Longitudinal (w_z) and horizontal (w_r) droplet size as a function of ε_{dd}^{-1} for the same particle numbers as in (b). In (b) the vortex core size is defined as the distance from the origin to the point where the density reaches 90% of its maximum. In (c) the radial (axial) width is defined as the mean length $w_{r(z)} \equiv (w_i + w_e)/2$, where w_i and w_e are the distances between the points where the density reaches, respectively, 90% and 10% of its maximum value along the radial direction (along the vertical, peak-density line). In all panels lines are variational results, and dots are numerical results for stationary solutions of Eq. (1), imposing a vortex with azimuthal symmetry (see text).

is the dipolar potential. $C_{dd} = \mu_0 \mu^2 \equiv \frac{12\pi\hbar^2}{m} a_{dd}$ is the dipolar coupling constant, μ is the magnetic dipole moment, θ is the angle between $\mathbf{r}$ and the vertical axis (polarization axis of the dipoles), and $a_{dd} = \frac{\mu_0\mu^2 m}{12\pi\hbar^2}$ is the dipolar length. The parameter $\varepsilon_{dd} = a_{dd}/a_s$ is the ratio of dipolar interaction to the s-wave interaction strengths, defining stability of a uniform condensate in the Bogoliubov approach when $\varepsilon_{dd} < 1$ [5]. Quantum fluctuation corrections to the mean-field energy for a uniform dipolar condensate are introduced in Eq. (1) by a Lee-Huang-Yang–type (LHY) term, with coefficient $g_{LHY} = \frac{128\sqrt{\pi}}{3} \frac{\hbar^2 a_s^{5/2}}{m}(1 + \frac{3}{2}\varepsilon_{dd}^2)$ [27,28,49]. Energetic stability of dipolar droplets in trapping potentials have been studied in a number of works. A stability diagram for droplets in free space was proposed in [26] via a Gaussian ansatz and checked against numerical simulations. The variational approach well describes collective properties of the condensate, such as the energy, the shape close to the instability region, and excitation spectra [29].

III. ENERGETIC STABILITY DIAGRAM

We begin our study with the static properties of vortex lines introducing a variational wave function

$$\psi_V(\mathbf{r}) = \left(\frac{2^{2\ell+3}N}{\pi^{\frac{3}{2}}\sigma_\rho^{2\ell+2}\sigma_z}\right)^{\frac{1}{2}} \rho^\ell\, e^{i\ell\phi}\, e^{-2\left(\frac{\rho^2}{\sigma_\rho^2} + \frac{z^2}{\sigma_z^2}\right)}, \quad (2)$$

where N is the particle number and ρ the radial coordinate [50]. The choice $\ell = 0$ corresponds to a state with no vortex, whereas for $\ell > 0$ the state has ℓ quanta of circulation. In this work we specialize to the case of $\ell = 1$ and leave the investigation of multicharged vortices to a separate study. In Eq. (2) the widths of the condensate σ_ρ and σ_z are variational parameters to be determined via a minimization of the full energy functional associated with Eq. (1). Therefore, we compute the rescaled

energy

$$\frac{E_V}{E_0} = \frac{1}{N\sigma_z^2}\left(1 + \frac{4}{y^2}\right) + \frac{2\sqrt{2}}{\pi^{\frac{1}{2}}\sigma_z^3 y^2 N}\left(\varepsilon_{dd}^{-1} - g(y)\right)$$
$$+ \frac{8192\sqrt{2}}{625\pi^{5/4}}\frac{1 + \frac{3}{2}\varepsilon_{dd}^2}{\varepsilon_{dd}^{5/2} N^2}, \quad (3)$$

where $E_0 = \frac{\hbar^2}{m\, a_{dd}^2}$, $y = \sigma_\rho/\sigma_z$, $g(x) = f(x) + 3x\, f'(x)/8 + x^2\, f''(x)/8$, and $f(x) = \frac{1+2x^2}{1-x^2} - \frac{3x^2 \text{arctanh}\sqrt{1-x^2}}{(1-x^2)^{3/2}}$ [5]. The resulting minimization of Eq. (3) is shown in Fig. 1(a) as a function of ε_{dd}^{-1} and particle number N. For comparison we show the result of energy minimization for $\ell = 0$ (dashed line) [26]. The shaded region below the full line is the energetic stability region of a droplet with $\ell = 1$, which is shrunk compared to the $\ell = 0$ case. Above the solid line there is no minimum, and the minimum energy state is a uniform solution with vanishing density [51].

IV. SHAPE OF DIPOLAR DROPLETS WITH A VORTEX LINE

We proceed by characterizing the shape of the droplet in the presence of a vortex for different particle numbers and ε_{dd}. In Fig. 1(b) we compute the vortex core size in units of a_{dd}, whereas in Fig. 1(c) we plot the horizontal and vertical widths w_r and w_z. The vortex core size is defined from the origin over the $z = 0$ plane to the point where the density reaches 90% of its maximum value. The droplet radial (axial) width is defined as the mean length $w_{r(z)} = (w_i + w_e)/2$, where w_i and w_e are the distances between the points where the density reaches, respectively, 90% and 10% of its maximum value along the radial direction (along the vertical, peak-density line). Variational calculations are checked against full numerical simulations of Eq. (1) in imaginary time (dots in Fig. 1), exploiting the azimuthal symmetry of vortex states,
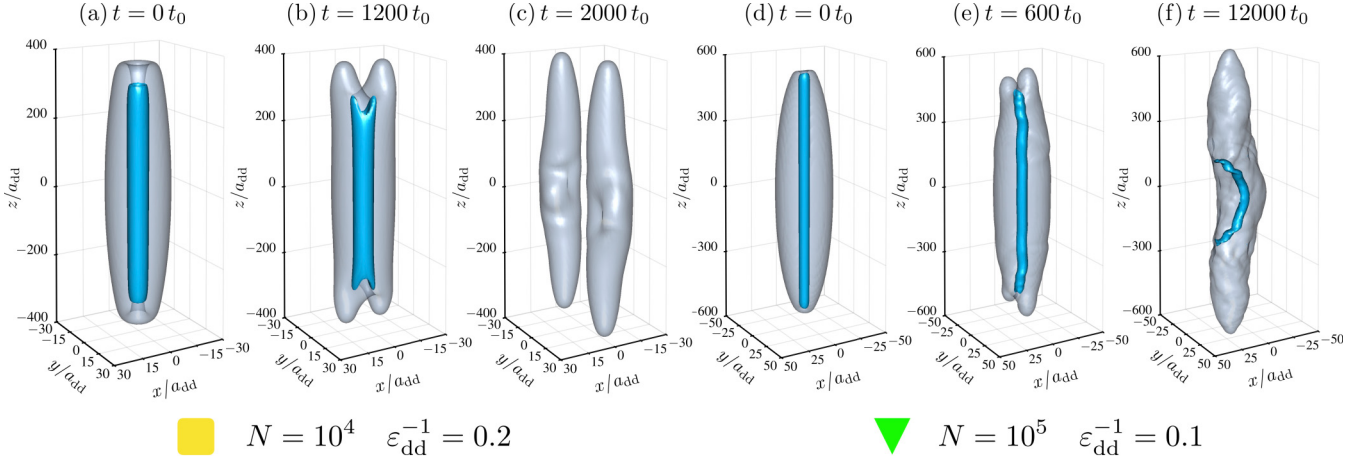
FIG. 2. Real-time dynamics of droplets with vortex lines. (a), (b), (c) Splitting instability for $N = 10^4$ particles and $\varepsilon_{dd}^{-1} = 0.2$. Snapshots of the dynamics at $t/t_0 = 0, 1200, 2000$, where $t_0 = m\,a_{dd}^2/\hbar$. At intermediate time $t = 1200\,t_0$ droplets split in two fragments moving at a finite (opposite) momentum and carry excitations with finite angular momentum. (d), (e), (f) Vortex-line bending for $N = 10^5$ and $\varepsilon_{dd}^{-1} = 0.1$. Snapshots of the dynamics at $t/t_0 = 0, 600, 12\,000$. At initial times unstable Kelvin-wave modes tend to split the droplet. After a transient dynamics, where part of the angular momentum is transferred to surface collective excitations, the vortex line bends ($t = 12\,000\,t_0$). See the full-dynamics video in the Supplemental Material [68]. Notice the difference in the length scales between the axes of the $N = 10^4$ and $N = 10^5$ plots due to very strong anisotropy and different droplet lengths. Results are obtained by solving numerically Eq. (1) on a grid size of $512 \times 512 \times 256$ points.

where we assume $\psi_V(\mathbf{r}) = e^{i\phi}\Psi_V(\rho, z)$. The problem reduces then to an effective two-dimensional (2D) problem for the function $\Psi(\rho, z)$ (solved over a grid size of 512×256 points). To efficiently compute the kinetic term, we employ a discrete Hankel transform in the radial direction (of first order, to impose the vortex node at $\rho = 0$) and the usual fast Fourier transform in the longitudinal direction [52]. In Figs. 1(b) and 1(c) lines terminate at the spinodal point of Fig. 1(a) for the corresponding value of N. We notice that for a wide range of interactions and particle numbers the vortex core is of the same order of the radial width w_r, and both are always much smaller than the longitudinal width w_z. All lengths decrease slightly by increasing ε_{dd} for a fixed N. For every simulation analyzed in Fig. 1, both ρ and z domains were chosen to be at least twice as large as the maximum extension of the droplet predicted by the variational approach (i.e., $\gtrsim 2\,\sigma_z$). The application of an interaction cutoff (as proposed in [53]) turned out to be irrelevant in these large-domain cases, meaning that the Fourier copies (of the periodically bound numerical box) were sufficiently spaced, making artificial effects of the long-range interaction negligible. We observe agreement between the variational and numerical results for small ε_{dd} and particle numbers. A discrepancy for large particle numbers and stronger interactions [as is the case of $\varepsilon_{dd}^{-1} < 0.2$ and $N = 10^5$, see Fig. 1(b)] is expected due to the combined effect of the limited validity of the variational ansatz as well as for resolution issues related to the strong anisotropy of the droplet.

V. REAL-TIME DYNAMICS

A crucial issue, relevant for the experiments, is the stability of such vortex states in self-bound droplets. To address this point we perform fully three-dimensional simulations in real time to take into account possible instabilities which can break azimuthal symmetry (see below). The input states at $t = 0$ are

created from the results of 2D imaginary-time relaxation described previously. These 2D solutions are interpolated to a grid of $512 \times 512 \times 256$ points, thus generating three-dimensional initial states [see Figs. 2(a) and 2(d)], slightly perturbed with numerical noise.

In Fig. 2 we illustrate the prototypical real-time dynamics of a droplet with a vortex line at $t = 0$ for two cases of condensates of $N = 10^4$ and $N = 10^5$ particles with $\varepsilon_{dd}^{-1} = 0.2$ and 0.1, respectively. Time is measured in units of $t_0 = m\,a_{dd}^2/\hbar$, which equals $0.12\ \mu s$ for ^{164}Dy and $0.03\ \mu s$ for ^{168}Er. The blue shaded region is an isosurface cut of the magnitude of the pseudovorticity vector $\boldsymbol{\omega} = \nabla\,\mathrm{Re}(\psi) \times \nabla\,\mathrm{Im}(\psi)$. This quantity is tangent to the vortex line along its length and can be used to track the numerical points corresponding to the vortex core, where the zeros of the imaginary and real parts of the wave function intersect [54]. The two dynamics display very different features. For $N = 10^4$ the system develops a splitting instability and divides in two droplets with $N_f \approx N/2$ at $t \approx 1200\,t_0$, where N_f is the particle number of each droplet after splitting. For longer times the two fragments move apart with opposite momenta and display no residual vorticity. All initial angular momentum gets transferred into collective surface excitations of the droplets. For the larger system, splitting instability starts to develop at the same time $t = 600\,t_0$; however, the droplet does not fragment. At later times the condensate restores a dropletlike configuration with the development of Kelvin waves along the vortex line, eventually leading to vortex bending for $t = 12\,000\,t_0$ and surface excitations. We observe similar features, i.e., absence of splitting and enhancement of surface excitations, also for longer times. The shape of the bent vortex line resembles the U-shaped excitations studied in [55], which were shown to hold less angular momentum than a straight-line vortex state, corroborating our description of angular momentum being transferred to surface modes [see Fig. 2(f)]. Since external torques on the droplet are absent,
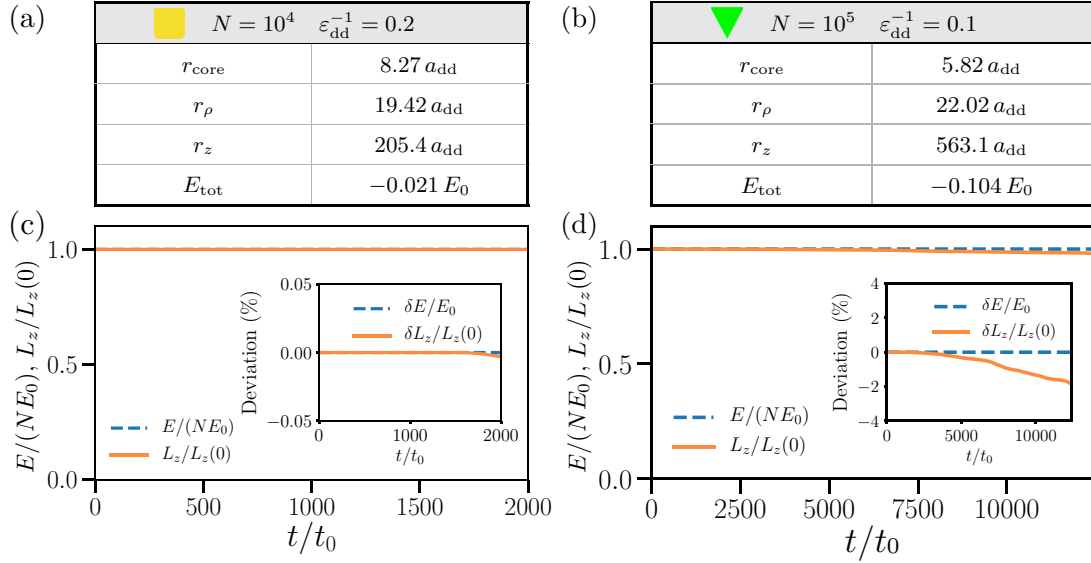
FIG. 3. Numerical simulations. Tables (a) and (b) show the vortex core r_{core}, the longitudinal r_z, and the transverse radius r_ρ in units of a_{dd} and the total energy per particle in units of E_0 for the two points in the diagram of Fig. 1. They correspond to the stationary state for (a) $N = 10^4$ and $\varepsilon_{\text{dd}}^{-1} = 0.2$, and (b) $N = 10^5$ and $\varepsilon_{\text{dd}}^{-1} = 0.1$. Results are obtained by solving numerically Eq. (1) with imaginary-time evolution on a grid as large as 512×256 points along the transverse and longitudinal directions, respectively. The domain ranges are (a) $\rho \times z \in [-300, 300] \times [-800, 800]$ and (b) $\rho \times z \in [-400, 400] \times [-1000, 1000]$ in units of a_{dd}. Plots (c) and (d) show the energy and longitudinal angular momentum conservation along the dynamics of Fig. 2 for the same particle numbers and interactions as in (a) and (b), respectively.

no change of the angular momentum along any direction is expected. Its necessary conservation means that angular momentum had to be transferred from the vortex line to surface modes. Numerically, a finer grid and larger simulation box would be needed in order to preserve the angular momentum along the vertical direction for very long times. In Figs. 3(c) and 3(d) we show the numerical deviation of the energy and longitudinal angular momentum for the two cases discussed above.

VI. EXPERIMENTAL CONSIDERATIONS

Vortices in ultracold atomic systems are controllably created either by phase imprinting or via an effective rotating potential generated by an applied laser beam. In any case, vortex imprint must be done in-trap, following the droplet preparation and before its release. The "optical spoon" technique is more invasive and requires longer equilibration times and it becomes less likely to work experimentally. Phase imprinting, on its turn, can be done with high spatial resolution as well as by means of very short optical pulses, allowing an almost instantaneous imprint of a vortex. Following the simulations presented above, the typical times for the observation of vortex dynamics for ^{164}Dy range from 100 μs to just below 2 ms, which is short but still within experimental resolution. For example, for the parameters as in Fig. 2(a), splitting instability sets on for times $t \approx 10^3 t_0$, which correspond to $t \approx 0.1$ ms for ^{164}Dy. Nevertheless, we have also verified instances in which the onset of the splitting process took slightly longer time. This was the case of $\varepsilon_{\text{dd}}^{-1} = 0.6$ and $N = 10^5$, where $t \approx 45\,000 \, t_0$, corresponding to $t \approx 6$ ms. Detection, in any case, must be done *in situ*, preferably with a levitating external magnetic field gradient to allow for longer observation times [21]. Extraction of dynamical properties, e.g., momentum, shape, atom number,

and/or absence of droplet movement in the cases covered in Fig. 2, can be done at longer evolution times, on the order of several milliseconds, when detection is expected to be easier.

VII. CONCLUSIONS

In this article we studied the stability of quantum vortex lines in dilute self-bound droplets of dipolar atoms. We first discussed the energetic stability region of such vortex excitations via a variational ansatz in the generalized nonlocal Gross-Pitaevskii functional that includes a LHY-type contribution. The region corresponding to the stationary solutions where $E_V < 0$ is unstable to fragmentation into two droplets. When this is not the case we found that Kelvin waves establish along the vortex line, which eventually bends in the central region of the droplet. We confirmed our findings by detailed fully three-dimensional numerical simulations of vortex states created by phase imprinting. The situation where Kelvin waves start developing has also been predicted to appear in a similar context of three-dimensional dipolar BECs [11]. Droplets with vortices may thus serve as promising test-beds to the study of twisted vortex lines in real-life experiments. An extension of this work would include the investigation of the excitation spectrum of these vortex lines, similarly to what has been recently done in vortex-free droplets [30], and with vortex states in trapped geometries [56]. These instabilities offer new opportunities for devising stabilization methods, such as temporal or spatial modulation of the scattering length as proposed for nondipolar BECs [57,58] or pinning potentials [59,60]. Also, the appearance of vortex arrays [61,62] as well as the effects of impurities and turbulence phenomena may be relevant to current experiments [63–66].

[1] A. Fetter and A. Svidzinsky, J. Phys.: Condens. Matter **13**, R135 (2001).

[2] F. Dalfovo and S. Stringari, J. Chem. Phys. **115**, 10078 (2001).

[3] K. W. Madison, F. Chevy, W. Wohlleben, and J. Dalibard, Phys. Rev. Lett. **84**, 806 (2000).

[4] M. W. Zwierlein, J. R. Abo-Shaeer, A. Schirotzek, C. H. Schunck, and W. Ketterle, Nature (London) **435**, 1047 (2005).

[5] T. Lahaye, C. Menotti, L. Santos, M. Lewenstein, and T. Pfau, Rep. Prog. Phys. **72**, 126401 (2009).

[6] A. M. Martin, N. G. Marchant, D. H. J. O'Dell, and N. G. Parker, J. Phys.: Condens. Matter **29**, 103004 (2017).

[7] M. Abad, M. Guilleumas, R. Mayol, M. Pi, and D. M. Jezek, Phys. Rev. A **79**, 063622 (2009).

[8] I. Tikhonenkov, B. A. Malomed, and A. Vardi, Phys. Rev. A **78**, 043614 (2008).

[9] R. M. Wilson, S. Ronen, J. L. Bohn, and H. Pu, Phys. Rev. Lett. **100**, 245302 (2008).

[10] W. E. Shirley, B. M. Anderson, C. W. Clark, and R. M. Wilson, Phys. Rev. Lett. **113**, 165301 (2014).

[11] M. Klawunn, R. Nath, P. Pedri, and L. Santos, Phys. Rev. Lett. **100**, 240403 (2008).

[12] M. Klawunn and L. Santos, New J. Phys. **11**, 055012 (2009).

[13] F. Dalfovo, S. Giorgini, L. P. Pitaevskii, and S. Stringari, Rev. Mod. Phys. **71**, 463 (1999).

[14] N. Navon, S. Piatecki, K. Günter, B. Rem, T. C. Nguyen, F. Chevy, W. Krauth, and C. Salomon, Phys. Rev. Lett. **107**, 135301 (2011).

[15] N. Navon, S. Nascimbène, F. Chevy, and C. Salomon, Science **328**, 729 (2010).

[16] H. Kadau, M. Schmitt, M. Wenzel, C. Wink, T. Maier, I. Ferrier-Barbut, and T. Pfau, Nature (London) **530**, 194 (2016).

[17] I. Ferrier-Barbut, H. Kadau, M. Schmitt, M. Wenzel, and T. Pfau, Phys. Rev. Lett. **116**, 215301 (2016).

[18] L. Chomaz, S. Baier, D. Petter, M. J. Mark, F. Wächtler, L. Santos, and F. Ferlaino, Phys. Rev. X **6**, 041039 (2016).

[19] I. Ferrier-Barbut, M. Schmitt, M. Wenzel, H. Kadau, and T. Pfau, J. Phys. B **49**, 214004 (2016).

[20] M. Schmitt, M. Wenzel, B. Boöttcher, I. Ferrier-Barbut, and T. Pfau, Nature (London) **539**, 259 (2016).

[21] M. Wenzel, F. Böttcher, T. Langen, I. Ferrier-Barbut, and T. Pfau, Phys. Rev. A **96**, 053630 (2017).

[22] L. Chomaz et al., Nat. Phys. **14**, 442 (2018).

[23] C. R. Cabrera, L. Tanzi, J. Sanz, B. Naylor, P. Thomas, P. Cheiney, and L. Tarruell, Science **359**, 301 (2018).

[24] D. S. Petrov, Phys. Rev. Lett. **115**, 155302 (2015).

[25] D. S. Petrov and G. E. Astrakharchik, Phys. Rev. Lett. **117**, 100401 (2016).

[26] D. Baillie, R. M. Wilson, R. N. Bisset, and P. B. Blakie, Phys. Rev. A **94**, 021602(R) (2016).

[27] F. Wächtler and L. Santos, Phys. Rev. A **93**, 061603 (2016).

[28] R. N. Bisset, R. M. Wilson, D. Baillie, and P. B. Blakie, Phys. Rev. A **94**, 033619 (2016).

[29] F. Wächtler and L. Santos, Phys. Rev. A **94**, 043618 (2016).

[30] D. Baillie, R. M. Wilson, and P. B. Blakie, Phys. Rev. Lett. **119**, 255302 (2017).

[31] F. Cinti and M. Boninsegni, Phys. Rev. A **96**, 013627 (2017).

[32] A. Macia, J. Sánchez-Baena, J. Boronat, and F. Mazzanti, Phys. Rev. Lett. **117**, 205301 (2016).

[33] F. Cinti, A. Cappellaro, L. Salasnich, and T. Macrì, Phys. Rev. Lett. **119**, 215302 (2017).

[34] H. Saito, J. Phys. Soc. Jpn. **85**, 053001 (2016).

[35] A. Boudjemâa, Ann. Phys. **381**, 68 (2017).

[36] D. Laghi, T. Macrì, and A. Trombettoni, Phys. Rev. A. **96**, 043605 (2017).

[37] A. Cappellaro, T. Macrì, G. F. Bertacco, and L. Salasnich, Sci. Rep. **7**, 13358 (2017).

[38] For similar results that include the stabilization via nondissipative three-body interactions see, e.g., S. K. Adhikari, Laser Phys. Lett. **14**, 025501 (2017); Phys. Rev. A **95**, 023606 (2017).

[39] L. F. Gomez, K. R. Ferguson, J. P. Cryan, C. Bacellar, R. M. P. Tanyag, C. Jones, S. Schorb, D. Anielski, A. Belkacem, C. Bernando et al., Science **345**, 906 (2014).

[40] F. Dalfovo, R. Mayol, M. Pi, and M. Barranco, Phys. Rev. Lett. **85**, 1028 (2000).

[41] K. K. Lehmann and R. Schmied, Phys. Rev. B **68**, 224520 (2003).

[42] F. Ancilotto, M. Pi, and M. Barranco, Phys. Rev. B **91**, 100503(R) (2015).

[43] F. Ancilotto, M. Barranco, F. Coppens, J. Eloranta, N. Halberstadt, A. Hernando, D. Mateo, and M. Pi, Int. Rev. Phys. Chem. **36**, 621 (2017).

[44] H. Saito and M. Ueda, Phys. Rev. Lett. **89**, 190402 (2002).

[45] A. Aftalion and T. Riviere, Phys. Rev. A **64**, 043611 (2001).

[46] J. J. García-Ripoll and V. M. Pérez-García, Phys. Rev. A **64**, 053611 (2001).

[47] V. Bretin, P. Rosenbusch, F. Chevy, G. V. Shlyapnikov, and J. Dalibard, Phys. Rev. Lett. **90**, 100403 (2003).

[48] T. P. Simula, T. Mizushima, and K. Machida, Phys. Rev. Lett. **101**, 020402 (2008).

[49] A. R. P. Lima and A. Pelster, Phys. Rev. A **84**, 041604(R) (2011).

[50] R. P. Teles, F. E. A. dos Santos, M. A. Caracanhas, and V. S. Bagnato, Phys. Rev. A **87**, 033622 (2013).

[51] We checked from the variational ansatz that metastable solutions for which a local minimum has positive energy exist and are within the width of the black solid line.

[52] The Hankel transform of a function $f(\rho, z)e^{i\ell\phi}$ is given by $\tilde{f}(k_\rho, k_\phi, z) = -2i\pi \int_0^\infty f(\rho, z)J_1(k_\rho\rho)\rho d\rho$. The full momentum-space representation of $f(\rho, z)e^{i\ell\phi}$ is then $\tilde{f}(\mathbf{k}) = \mathcal{F}_z[\tilde{f}(k_\rho, k_\phi, z)]$, with $\mathcal{F}_z[\cdot]$ the usual Fourier transform

along the z direction. See [56] for further details on the algorithm.

[53] H. Y. Lu, H. Lu, J. N. Zhang, R. Z. Qiu, H. Pu, and S. Yi, Phys. Rev. A **82**, 023622 (2010).

[54] S. Serafini, L. Galantucci, E. Iseni, T. Bienaimé, R. N. Bisset, C. F. Barenghi, F. Dalfovo, G. Lamporesi, and G. Ferrari, Phys. Rev. X **7**, 021031 (2017).

[55] A. Aftalion and I. Danaila, Phys. Rev. A **68**, 023603 (2003).

[56] R. M. Wilson, S. Ronen, and J. L. Bohn, Phys. Rev. A **79**, 013621 (2009).

[57] F. K. Abdullaev, J. G. Caputo, R. A. Kraenkel, and B. A. Malomed, Phys. Rev. A **67**, 013605 (2003).

[58] S. K. Adhikari, Phys. Rev. A **69**, 063613 (2004).

[59] T. Isoshima and K. Machida, Phys. Rev. A **59**, 2203 (1999).

[60] P. Kuopanportti, J. Low Temp. Phys. **161**, 561 (2010).

[61] N. R. Cooper, E. H. Rezayi, and S. H. Simon, Phys. Rev. Lett. **95**, 200402 (2005).

[62] J. Zhang and H. Zhai, Phys. Rev. Lett. **95**, 200403 (2005).

[63] C. F. Barenghi, L. Skrbek, and K. R. Sreenivasan, Proc. Natl. Acad. Sci. USA **111**, 4647 (2014).

[64] M. C. Tsatsos, P. E. S. Tavares, A. Cidrim, A. R. Fritsch, M. A. Caracanhas, F. E. A. dos Santos, C. F. Barenghi, and V. S. Bagnato, Phys. Rep. **622**, 1 (2016).

[65] M. Tsubota, K. Fujimoto, and S. Yui, J. Low Temp. Phys. **188**, 119 (2017).

[66] T. Bland, A. W. Baggaley, and N. G. Parker, arXiv:1706.02660.

[67] G. R. Dennis, J. J. Hope, and M. T. Johnsson, Comput. Phys. Commun. **184**, 201 (2013).

[68] See Supplemental Material at http://link.aps.org/supplemental/10.1103/PhysRevA.98.023618 for the full dynamics.